

PAPER • OPEN ACCESS

Aztec shape metamaterial-based bandpass filter for C, X and Ku-band applications

To cite this article: M J Alam *et al* 2019 *IOP Conf. Ser.: Earth Environ. Sci.* **228** 012019

View the [article online](#) for updates and enhancements.

Aztec shape metamaterial-based bandpass filter for C, X and Ku-band applications

M J Alam¹, E Ahamed¹, M R I Faruque^{1*}, M J Hossain¹, M T Islam²

1 Space Science Centre (ANGKASA), Institute of Climate Change (IPI), Universiti Kebangsaan Malaysia, 43600 Bangi, Selangor, Malaysia.

2 Centre of Advanced Electronic and Communication Engineering, Universiti Kebangsaan Malaysia, 43600 Bangi, Selangor, Malaysia.

rashed@ukm.edu.my

Abstract. The paper presents the structure of an Aztec shape metamaterial unit cell that is suitable for a triple band of microwave frequencies. A comparative analysis has been made on the performance of the unit cell with several array structures. A low profile dielectric substrate FR-4 is used on which the design is made. The proposed structure operates at 6.3, 8.9, 11.91, and 16.42 GHz respectively. The double negative characteristics can also be found at X and Ku-band separately. Having a compact design, double-negative characteristics and the proposed metamaterial has potential to be used for triple band applications, especially for C, X and Ku-band.

1. Introduction

Before 1968, it was quite impossible to use an engineered material for the purpose of designing. Veselago et al [1] had made it possible and shown the world the impact of the artificial material. The materials that are found in nature do not have the power to control the electromagnetic properties. However, negative permittivity (ϵ) and permeability (μ) in a material characteristic was a myth for everyone. Thus the use of metamaterial had come into play. The unconventional structure, power to control the electromagnetic wave beams and negative effective parameters have made the metamaterial superior to any other materials found in nature.

Metamaterial is an artificially engineered composite material that exhibits some exotic electromagnetic properties and overcomes the usual limitations of natural available materials. These extraordinary properties of metamaterial may include negative permittivity, negative permeability, inverted Snell's law and some other similar reverse electromagnetic phenomena. After the first successful invention of metamaterial by Smith and his colleagues (Smith et al. 2000), it is being utilized in almost all the applications of electromagnetism due to these exciting electromagnetic properties.

Having these unorthodox and exceptional characteristics, metamaterials can be used in cloaking [2], filters [3], design of antenna [4], super lenses [5], reduction of SAR, absorber and electromagnetic band gaps etc. In some cases, intrinsic negative permittivity is found. Different alphabetic shapes have become popular for particular operations [7]; for instance, Benosman et al. [8] introduced a double S-



shaped metamaterial that showed negative values of η between 15.67 - 17.43GHz. Another research group proposed various U-shaped rectangular array structures left-handed aspect at approximately 5, 6 and 11GHz. A V-shaped metamaterial showed double-negative characteristic. Zhou et al. designed an S-shaped $15 \times 15 \text{ mm}^2$ chiral metamaterial for X- and Ku-band application. Though the EMR was not higher than 4. For the purpose of application on S and C bands, Alam et al. [9] designed modified P-shaped DNG for different unit cells and array sizes. Even though multi-ban metamaterial absorbers is a promising application there have been few studies conducted focusing the design of this type of materials [10].

2. Design of the structure

The diagram of the prospective structure is itemized in Fig. 1. Here one side of the substrate is comprised of modified Aztec shape resonator with border on the edges. Each unit cell comprises with 11mm in length and 12mm in width. Copper is used as a metal element on FR4 substrate and metal element's thickness is 0.035mm and substrate thickness is 1.6mm. The dielectric constant of FR4 substrate is $\epsilon_r = 4.3$, a dielectric loss-tangent is $\tan\delta = 0.025$. Designed parameters of the proposed metamaterial are enlisted in Table 1. There 'a' and 'b' are the length and width of the proposed prototypes. The specification c is the Aztec shapes one arm length and d is the length of the other arm. Moreover, 'g' and 's' are same in dimension and one is the gap of split and another one is the resonator width respectively.

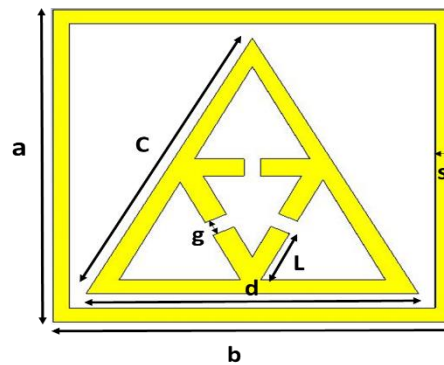


Fig. 1: Proposed Unit cell structure.

Table 1. Unit cell specification

Parameters	Dimension (mm)	Parameters	Dimension (mm)
a	11	c	10.30
b	12	d	10
s & g	0.5	L	1.48

3. Methodology

The reflection coefficient S11 named as a return loss and transmission coefficient S21 named as an insertion loss are extracted from the electromagnetic structure by using the CST Microwave Studio. The electromagnetic waves are generated using two waveguide ports and that waves are propagated through the filter configuration in Z-axis direction. The boundary condition for the metamaterial structure are applied as the perfect electric conductor (PEC) and perfect magnetic conductor (PMC) are in X- and Y- axis direction respectively. The frequency domain solver based simulator is used for

free-space simulation purpose. The unit cell act like a LC resonance circuit and its resonator indicated for the circuit is inductance and its split gap behaves like a capacitor. Therefore, by applying electromagnetic field it creates extraordinary properties. By increasing resonator width or gap inductance or capacitance will be varied properly. A flexible tetrahedral mesh is used for analyzing the proposed structure. The normalized impedance is set as 50ohm and the simulation is executed from 2 to 18GHz that is shown in Fig 2. To differentiate the effective permittivity (ϵ_r), permeability (μ_r) and refractive index (η_r) the NRW method is used. The effective permittivity and effective permeability are determined by the equation 1 and equation 2.

$$\epsilon_r = \frac{c}{j\pi f d} \times \frac{(1-V_1)}{(1+V_1)} \quad (1)$$

$$\mu_r = \frac{c}{j\pi f d} \times \frac{(1-V_2)}{(1+V_2)} \quad (2)$$

The effective refractive index (η_r) can defined by the equation 3.

$$\eta_r = \frac{c}{j\pi f d} \times \sqrt{\frac{(S_{21}-1)^2 - S_{11}^2}{(S_{21}+1)^2 - S_{11}^2}} \quad (3)$$

Where, f is the frequency, S_{21} and S_{11} are the insertion loss and return loss

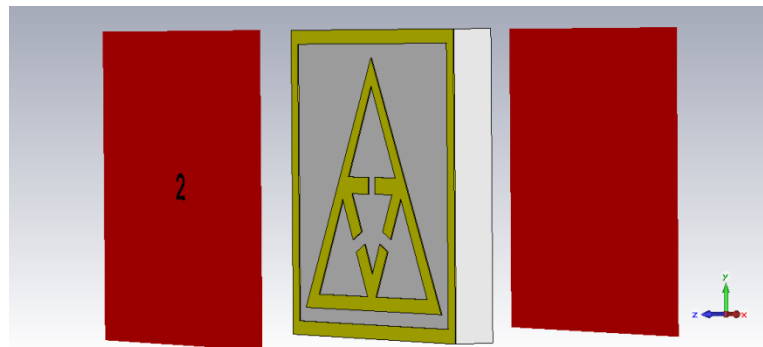


Fig. 2: Simulation set-up of unit cell structure.

4. Results and Discussions

4.1. Analyzing unit cell

The resonator based filter characterized by the scattering parameters. The scattering parameters reflection coefficient or return loss (S_{11}) and transmission coefficient or insertion loss (S_{21}) are seen in Figure 3. Unit cell, two by one array and two by two array are analyzed here for characterizing the structure. The unit cell shows pass band characteristics at 6.30 GHz, 8.90GHz, 11.91 GHz and 16.42 GHz with maximum attenuation of -12.95 dB, -12.95 dB, -18.04 dB and -28.33 dB respectively.

The effective parameters are shown in Figure 3 (b) for the simulated unit cell structure. The FR4 substrate is used to design the filter with an area of 12×11 mm² for unit cell. Different types of methods are used to find out the effective parameters like Nicolson-Ross-Weir NRW methods, direct retrieval method of refractive index (DRI) methods etc. Moreover, main focused point for this work is based on the real values of the effective parameters that are retrieved from the return loss and insertion

loss. All of the cases for unit cell and array structures the results are showing the negative values for the operating frequency band in case of effective parameters. From the Figure 3 and Figure 5 determined negative values for the effective parameters are almost same for the unit cell structure and array structure. The negative permittivity are shown in figure 3 at 2- 4.13 GHz (bandwidth), 6.28-7.24 GHz, 8.88-10.57 GHz, 11.93-14.27 GHz and 14.99-15.92 GHz. The permeability shows negativity at 2-4.13 GHz, 8.86-15.40 GHz and 17.69- 18 GHz. The refractive index shows negativity at 7.48-8.93 GHz, 9.20-12 GHz and 12.28-16.34 GHz. And it shows double negative properties at 9.26 GHz with negative permittivity value -1.89, negative permeability value -24.94 and negative refractive index value -115.47.

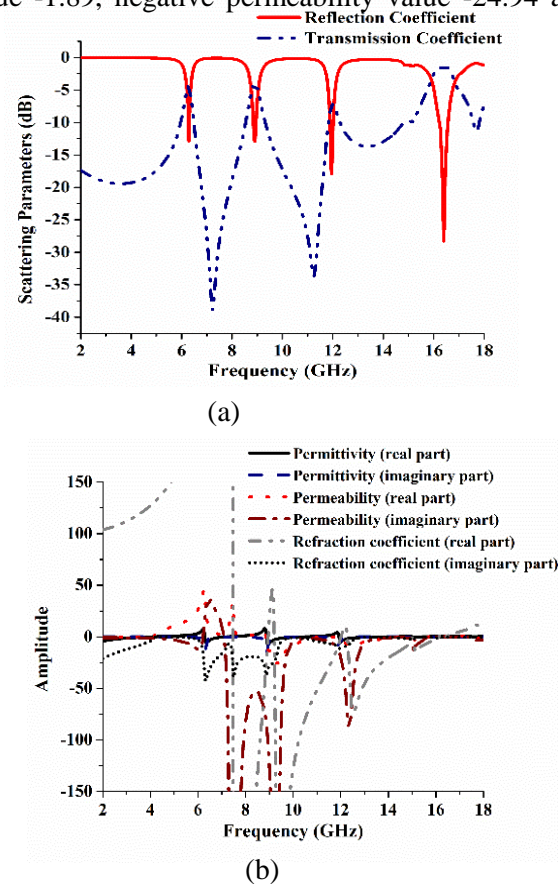


Fig. 3: Unit cell based simulated (a) return loss and insertion loss & (b) effective parameters (permittivity, permeability and refractive index) of the pass band filter.

Figure 4 indicate the situation of the proposed structure when electromagnetic field is applied along with electric field and magnetic field. Its electric field is shown in figure 4(a) where its maximum induced field indicated in the inner resonator's split gaps. Figure 4(b) represent the magnetic field where it induced in the outer resonator and figure 4(c) indicate the surface current distribution of the proposed passband structure.

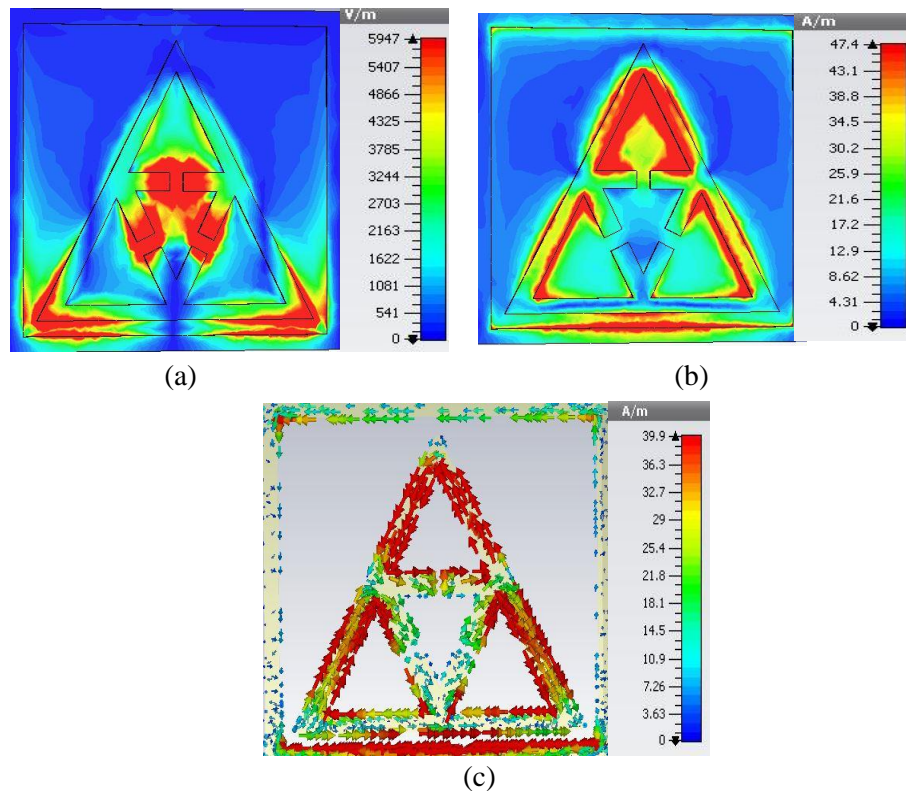


Fig. 4: Unit cell (a) electric field, (b) magnetic field & (c) surface current distribution at 9.26 GHz

4.2. Analyzing 2×1 array

The scattering parameters reflection coefficient or return loss (S11) and transmission coefficient or insertion loss (S21) are seen in figure 4. The two by one array structure shows the return loss resonances are at 6.33 GHz, 8.92GHz, 12.50 GHz and 16.52 GHz with maximum attenuation of -9.95 dB, -24.04 dB, -14.13 dB and -24.91 dB respectively. The negative permittivity are shown in figure 4 at 2- 4.16 GHz, 6.34-7.26 GHz, 8.92-10.71 GHz and 12.42-15.04 GHz. The permeability shows negativity at 7.49- 16.36 GHz. The refractive index shows negativity at 2-4.54 GHz, 8.90-12.16 GHz, 12.33- 14.31 GHz and 12.28-16.34 GHz. And it shows double negative properties at 9.26 GHz with negative permittivity value -5.44, negative permeability value -71.04 and negative refractive index value -23.53.

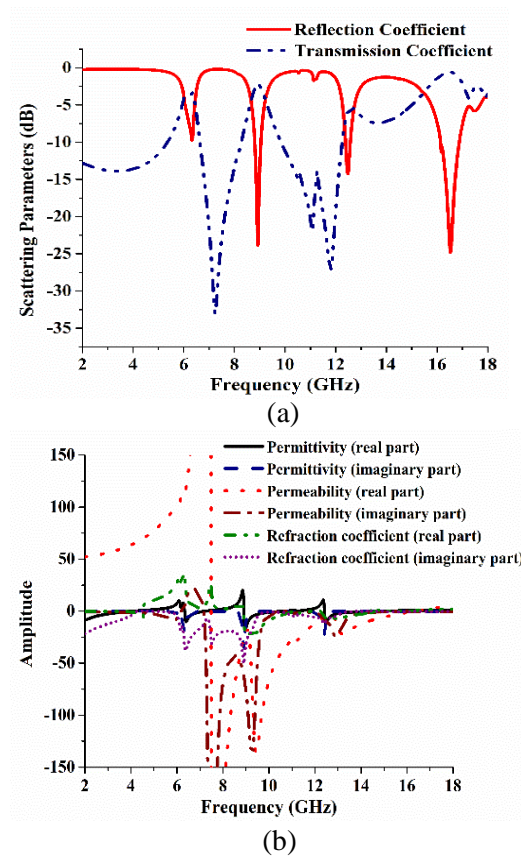
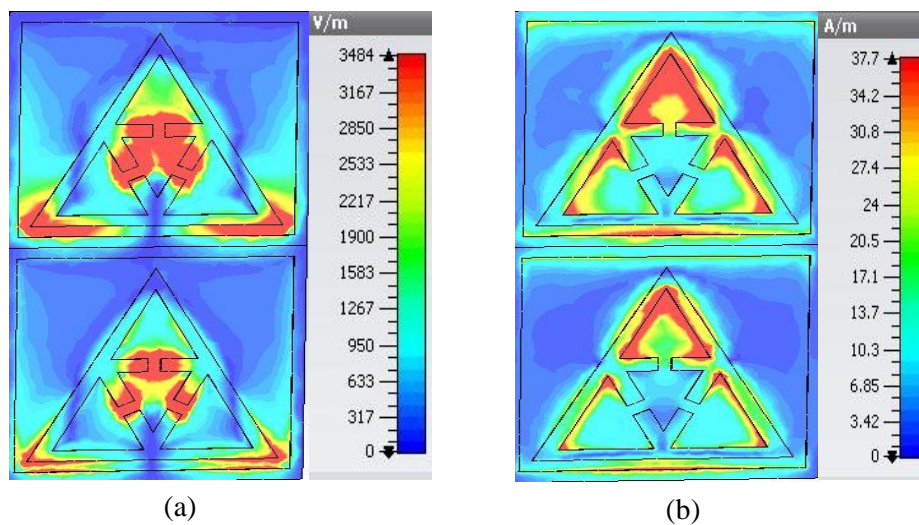
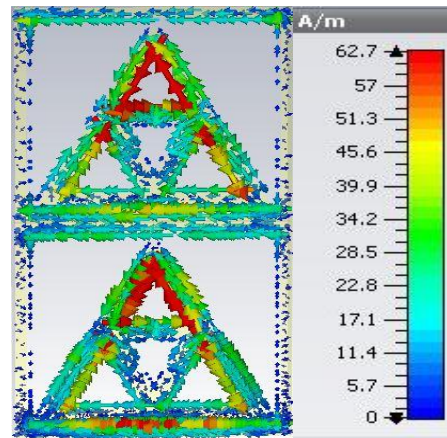


Fig. 5: 2×1 array based simulated (a) return loss and insertion loss & (b) effective parameters (permittivity, permeability and refractive index) of the passband filter.

Figure 6(a), 6(b) and 6(c) represent the electric field, magnetic field and surface current distribution at 9.26 GHz for the proposed 2×1 array structure. Where the electric field maximum concentrate in split gaps of Aztec structure and magnetic field induced in outer resonator of the structure. In the surface current distribution, currents are flowing in opposite directions between two resonators. So they cancel each other's effect and creating resonance frequency.



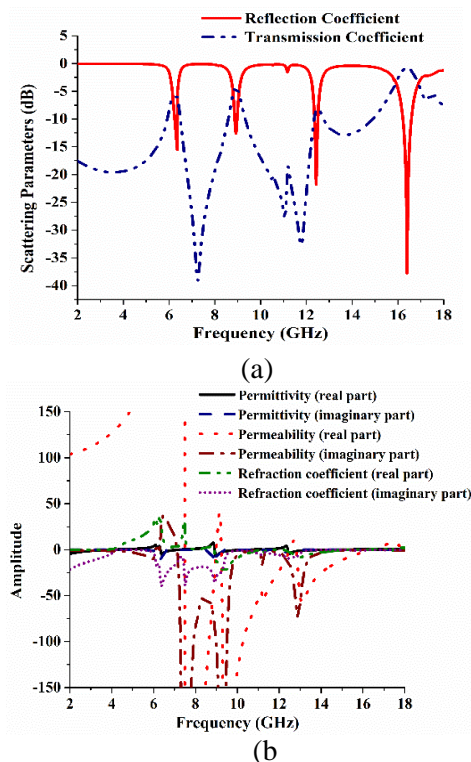


(c)

Fig. 6: 2×1 array (a) electric field, (b) magnetic field & (c) surface current distribution at 9.26 GHz

4.3. Analyzing 2×2 array

The scattering parameters reflection coefficient or return loss (S11) and transmission coefficient or insertion loss (S21) are seen in figure 5. The two by two array structure shows the return loss resonances are at 6.33 GHz, 8.92GHz, 12.44 GHz and 16.40 GHz with maximum attenuation of -15.55 dB, -12.57 dB, -21.95 dB and -37.71 dB respectively. The negative permittivity are shown in figure 3 at 2- 4.16 GHz (bandwidth), 6.34-7.28 GHz, 8.92-10.70 GHz and 12.41-15.13 GHz. The permeability shows negativity at 7.49-8.99 GHz, 9.24-12.42 GHz and 12.82-16.36 GHz. The refractive index shows negativity at 2-4.13 GHz, 8.90-14.86 GHz and 15.9-16.27 GHz. And it shows double negative properties at 9.26 GHz with negative permittivity value -2.70, negative permeability value -34.45 and negative refractive index value -20.92.



(b)

Fig. 7: 2×2 array based simulated (a) return loss and insertion loss & (b) effective parameters (permittivity, permeability and refractive index) of the passband filter

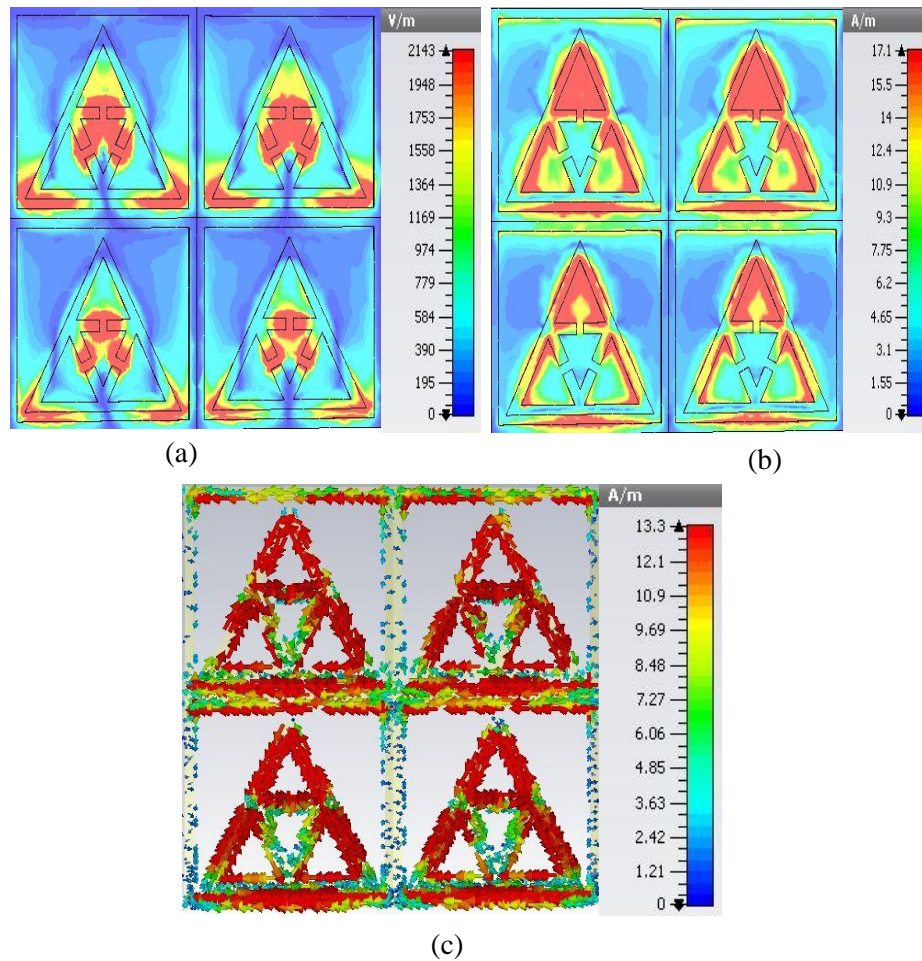


Fig. 8: 2×2 array (a) electric field, (b) magnetic field & (c) surface current distribution at 9.26 GHz.

Figure 8(a), 8(b) & 8(c) indicates the electric field, magnetic field and surface current distribution of the Aztec 2×2 array structure. Here also electric field induced in the split gaps of the inner structure and magnetic field induced in the outer resonator. The magnetic field depends on the current therefore, where the magnetic field induced concentration is maximum there the surface current concentration is high indicated by red colour in figure 8(c).

5. Conclusion

The proposed Aztec shaped pass band filter presents here with its different framework. The borders are embedded around the unit cell structure to create steadier operation through the whole unit cell at 6.30 GHz, 8.90GHz, 11.91 GHz and 16.42 GHz, respectively. The performance of the proposed filter structure is verified by its return loss, insertion loss, relative permittivity, and permeability. The overall performance and gain from the proposed filter is analysed analytically. Analytical resonating points are performed well by the effective parameters for the Aztec shaped filter. Its compact size, cost effectiveness and operative frequency range made that structure applicable. The proposed structure is potentially used as a band pass filter because of its appropriate architecture and its double negative characteristics.

6. References

- [1] Veselago V G 1968 *Sov Phys.* **10** 509.
- [2] Faruque M R I and Islam M T 2012 *Prog. Electromagn. Res.* **124** 119.
- [3] Islam M M, Islam M T, Samsuzzaman M and Faruque, M R I 2015 *Electron. Lett.*, **51** 1222.
- [4] Hasan M M, Faruque M R I. and Islam M T 2018 *Scientific Reports.* **8** 1-17.
- [5] Alam M J, Faruque M R I and Islam M T 2018 *J. Phys. D: App. Phys.* **51** 265102.
- [6] Islam S S, Faruque M R I. and Islam M T 2015 *AIP Advance.* **5** 107116.
- [7] Song K, Fu Q and Zhao X U 2011 *Phys Sci.* **84** 035402.
- [8] Huang Y, Wen J, Yang Y and Xie K *Appl Phys A.* **106** 79.
- [9] Benosman H and Hacene N B 2012 *Int J Comput Sci.* **9** 534.
- [10] Alam M J, Faruque M R I, Hossain M J and Islam M T 2018. *Mic. Opt. Tech. Lett.* **60** 1388.